

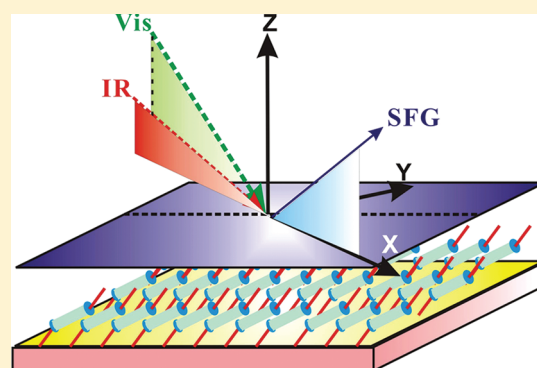
# Self Assembled Liquid Crystal Polymers on Photo-Irradiated Alignment Surfaces for Tailoring Response Properties of Liquid Crystal Molecules

Jung Y. Huang\* and Liu S. Li

Department of Photonics and Institute of Electro-Optical Engineering, Chiao Tung University, Hsinchu, Taiwan, R.O.C.

**S** Supporting Information

**ABSTRACT:** A liquid crystal polymer (LCP) self-assembled on a photo-irradiated substrate can modify the viscoelastic response of liquid crystal medium on the substrate. Sum-frequency vibrational spectroscopy shows that the phenyl groups of LCP are oriented epitaxially with layer thickness and an in-plane alignment order much higher than that at the photo-irradiated surface can be yielded. The liquid crystal molecules confined between the LCP-coated substrates reveals a stronger correlation among the thermally excited fluctuation modes. Our finding can be used to tailor the boundary forces on alignment substrates and to optimize the device performance.



## INTRODUCTION

Molecular alignment on surfaces or at an interface of two complex films has become an important issue in research. Information on molecular alignment could be useful for the fabrication of molecular devices for both optoelectronic and biosensing applications where improved alignment of interfacial molecules is highly desired. Long-range molecular ordering is also crucial to the activities of living organisms. This concept has inspired chemists to develop methods for tailoring molecular assemblies on a macroscopic scale for various device applications.<sup>1</sup>

In the case of liquid crystal (LC) devices, proper control of the optical response of liquid crystals with an electric field is required. To produce the functionality, researchers have employed mechanical buffing on a solid substrate to align LC molecules.<sup>2</sup> However, this mechanical contact process often causes the generation of dust and static charges on the surfaces of devices. In the past few years, new surface treatment techniques based on linearly polarized ultraviolet (LPUV) light<sup>3</sup> and an obliquely incident ion beam<sup>4</sup> have been developed to avoid aforementioned drawbacks and allow for patterning liquid crystal alignment. These noncontact alignment techniques, unfortunately, often yield an alignment surface with fairly weak anchoring strength, which often causes an image-sticking problem.

Manipulating surface forces to control molecular alignment in a device has been realized in some specific cases via photoisomerization effects.<sup>5,6</sup> Although the light-controlled alignment is highly attractive, prolonged irradiation with ambient light may erase the surface manipulation power. In this paper, we reported a different scheme to tailor the surface forces for aligning liquid crystal molecules and manipulating their dynamic response

properties. Our method involves only deposition of a thin liquid crystal polymer (LCP) on a LPUV-irradiated substrate. We employed sum-frequency vibrational spectroscopy (SFVS) to show that the surface anisotropy of the phenyl groups in the LPUV-irradiated RN1349 layer was printed on the LCP layer, and the resulting alignment order of the LCP phenyl rings were improved significantly. Dynamic light scattering (DLS) techniques were further employed to reveal that the viscoelastic properties of the LC molecules were changed by LCP on the LPUV-irradiated RN1349. Our results can also serve as the knowledge base for the development of patterned surfaces with controllable forces and allow engineers to optimize the performance of an optoelectronic device. This simple method could become greatly attractive in the future when the dimensions of LC containing devices are reduced to such a degree that the boundary conditions become an important issue.

## EXPERIMENTAL METHODS

The characterization of molecular alignments in a complex film and at a buried interface requires a combination of analytical techniques to provide the best characterization possible. Infrared-visible SFVS<sup>7</sup> offers both surface sensitivity and molecular specificity. Therefore, it was used first to probe the alignment anisotropy and order parameters in the LCP layers of various thicknesses on LPUV-irradiated substrates. Then, DLS techniques<sup>8</sup> were used to investigate the thermal fluctuation dynamic of LC molecules in LC devices with a variety of alignment surfaces.

**Received:** May 28, 2011

**Revised:** September 8, 2011

**Published:** September 08, 2011

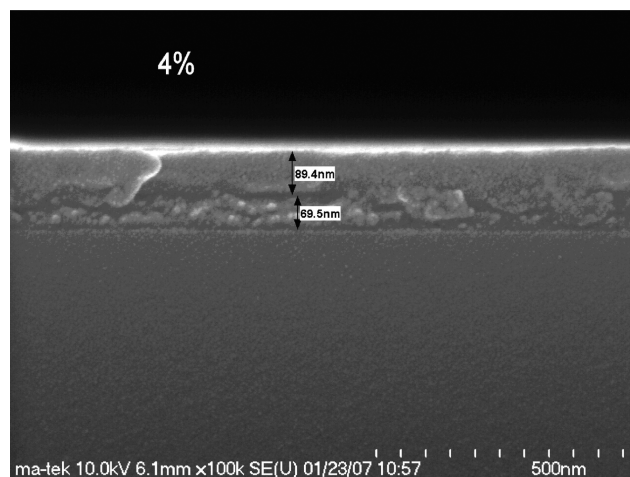


**Figure 1.** SEM micrograph showing the cross-section picture of LCP/RN1349/glass substrate prepared with 4% LCP solution.

**Materials and Sample Preparation.** The liquid crystals used for this study were E7 liquid crystals from Merck. We first coated indium tin oxide (ITO) glass substrates with RN1349 polyimide, which was specifically designed by Nissan Chemicals for non-contact LC photoalignment applications. We then irradiated the photoalignment layers with LPUV light at 365 nm to create an optic axis that was perpendicular to the polarization of the UV light. We spin-coated the substrates with a solution containing varying concentrations of LCP 1,4-phenylene bis(4-(6-(acryloyloxy) hexyloxy benzoate and cured the resulting LCP film by exposing it to unpolarized UV light. A scanning electron microscopic (SEM) micrograph of the cross-section picture of the resulting composite film was shown in Figure 1, with interfaces of the LCP/RN1349/glass clearly revealed. The thickness of the LCP layer can be easily controlled by varying the LCP concentration in the spin-coating solution and was determined with SEM, which yielded a calibration of thickness ( $t$ , in nm) versus LCP concentration ( $c$ , in %) as  $t = 13.5c + 30.8$ . A linear thickness control was achieved. However, the appearance of a nonzero constant indicates that we cannot reduce the layer thickness to zero by using an extremely dilute solution, presumably due to a preferential adsorption of LCP molecules onto the surface of RN1349.

To form a homogeneously aligned liquid crystal cell, the easy axes on both substrates were arranged to be antiparallel. Wedge cells were assembled by inserting spacers between the glass substrates at one side and allowing the other side to be in direct contact. We measured the thickness of the wedge cells with a cell gap inspection system RETS-3000 from Otsuka Electronics Co. Ltd. and the cell gap was found to vary from 0.9 to 3.0  $\mu\text{m}$ . We filled a test cell with E7 liquid crystals in an isotropic phase with a flow direction parallel to the easy axes of the substrates and then cooled the LC cells slowly to 25  $^{\circ}\text{C}$  to form a single nematic domain.

**Characterization Techniques.** *Infrared-Visible Sum-Frequency Vibrational Spectroscopy.* Experiments using infrared-visible SFVS<sup>9</sup> were carried out by employing a mode-locked picosecond Nd:YAG laser (Ekspla PL-2143, 35 ps, 10 Hz) with optical parametric generation and a difference frequency generation unit (Ekspla, PG401-DFG) to generate a tunable infrared (IR) pulse with a spectral resolution of 5  $\text{cm}^{-1}$ . We used the second harmonic pulse at 532 nm of the Nd:YAG laser output as an input visible beam. Typical input intensities were 300 and 100  $\mu\text{J}/\text{pulse}$  and incident angles were 45 $^{\circ}$  and 52 $^{\circ}$  for the visible and IR beams,

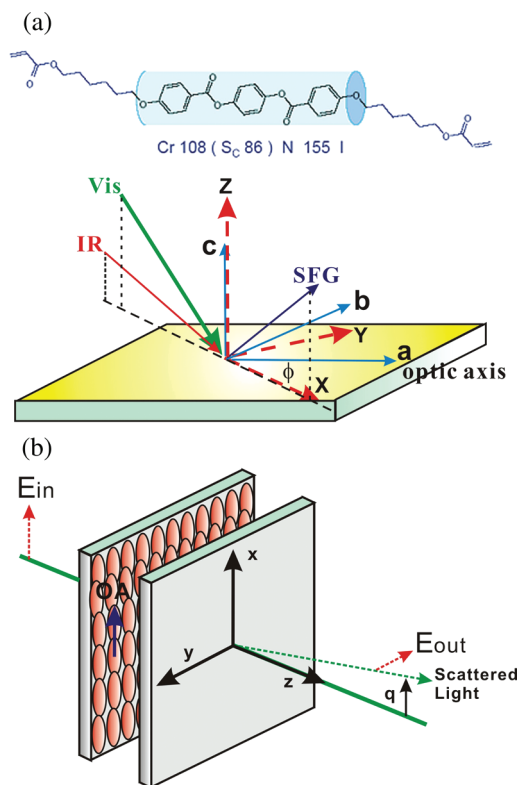


**Figure 2.** (a) Schematic angle-resolved SFVS depicting the relationship between the coordinate frames of the SFVS measurement ( $XYZ$ ) and LPUV-irradiated layer ( $abc$ ). The inset above shows the molecular structure of the 1,4-phenylene bis(4-(6-(acryloyloxy) hexyloxy benzoate of LCP moiety. The blue cylinder denotes the rod-like region of the LCP molecule. (b) Schematic of the DLS experimental geometry. Here OA denotes the optical axis of the LC film.

respectively. The visible and infrared beams were focused and overlapped at the surface of a sample (see Figure 2a). The sum frequency generation beam in reflection was filtered spatially with a series of apertures and spectrally with a short-pass filter (Omega Optical, third 500SP), and then detected by a photomultiplier tube (PMT). The current pulse of the PMT was processed by a preamplifier (Ortec 9305) and integrated using a boxcar averager (Stanford Research Systems). We acquired SFVS spectra by using  $ppp$  and  $ssp$  polarization combinations, where the letters indicate the polarizations of the SF, visible, and IR beams, respectively. All spectra were calibrated to the  $ssp$  signal from a z-cut LiNbO<sub>3</sub> at the same condition.

The SFVS signal is proportional to the square of the effective susceptibility tensor component projected from the molecular coordinate system to the laboratory frame. For example, the  $s$ -polarized sum-frequency optical field ( $\hat{e}_s^{\text{sf}}$ ) generated by  $s$ -visible ( $\hat{e}_s^{\text{v}}$ ) and  $p$ -infrared ( $\hat{e}_p^{\text{ir}}$ ) fields can be expressed as<sup>10,11</sup>

$$I_s(-\omega_{\text{sf}}; \omega_{\text{v}}, \omega_{\text{ir}}) / [I_s(\omega_{\text{v}}) I_p(\omega_{\text{ir}})] \propto |\chi_{ssp}^{(2)}(-\omega_{\text{sf}}; \omega_{\text{v}}, \omega_{\text{ir}})|^2$$

$$\text{with } \chi_{ssp}^{(2)}(-\omega_{\text{sf}}; \omega_{\text{v}}, \omega_{\text{ir}}) = \chi_{NR,ssp}^{(2)}(-\omega_{\text{sf}}; \omega_{\text{v}}, \omega_{\text{ir}})$$

$$+ \sum_Q \frac{A_{Q,ssp}}{\omega_{\text{ir}} - \omega_Q - i\gamma_Q}$$

$$\text{and } A_{Q,ssp} = N_s \int [\hat{e}_s^{\text{sf}} \cdot \vec{\alpha}_Q^{(2)} : \hat{e}_s^{\text{v}} \hat{e}_p^{\text{ir}}] f(\Omega) d\Omega \quad (1)$$

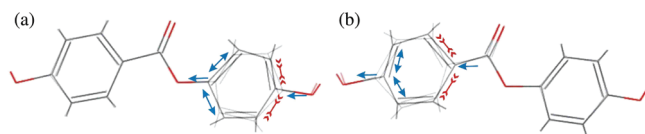


**Figure 3.** Normal-mode stretching patterns of the biphenyl carbonate moiety with normal-mode frequencies of 1503, and 1512  $\text{cm}^{-1}$ , respectively.

where  $A_{Q,ssp}$  is the resonant amplitude of the SFVS susceptibility with a resonant frequency  $\omega_Q$  and damping constant  $\gamma_Q$ .  $N_s$  is the surface density of the specific functional group  $q$ , and  $\alpha_Q^{(2)}$  denotes the nonlinear molecular polarizability, which relates to  $A_{Q,ssp}$  via an orientational average over a distribution  $f(\Omega)$ . For the calibration purpose, we derived the observed sum-frequency reference signal from a z-cut  $\text{LiNbO}_3$  to be  $|\tilde{\chi}_s^{(2)}(\text{LiNbO}_3)|^2 = 8000 \cdot [10^{-64} \text{ m}^2\text{C}^2/\text{V}^4]$  (see the Supporting Information S.1).

**Dynamic Light Scattering.** DLS is an effective technique to probe the thermally excited fluctuation of a thin-film material.<sup>8</sup> Typically, the methodology yields an autocorrelation function (ACF) of the scattering light intensity  $I_s(t)$  from the film. We used a He–Ne laser with a wavelength of 632.8 nm as the light source. The test cell was inserted in an optical setup with a crossed polarizer and analyzer. As illustrated in Figure 2b, we adjusted the incident light polarization to be along the optic axis of the test cell and adopted a forward scattering geometry with a scattering vector  $\vec{q}$  parallel to both the cells' substrates and the optic axis, corresponding to a scattering angle of  $\sim 10^\circ$ . This geometry ensures only azimuthal twist fluctuation to be observed and simplifies our DLS analysis. The scattered photons were detected with a silicon avalanche photodiode (SPCM-AQR-15, PerkinElmer) and then fed into the Flex02-01D digital correlator (Correlator.com) to calculate the intensity ACF in real time. The test LC cells in all measurements were kept at a specific temperature with  $\pm 0.1$  °C precision.

At finite temperature, the director  $\hat{n}$  of LC molecules constantly encounters a thermal fluctuation  $\delta \vec{n} = \hat{n} - \hat{n}_0$  from its equilibrium configuration  $\hat{n}_0$ . Two types of eigenmodes can be derived with the first originating from a mixed splay and bend deformation and the second with mixed twist and bend. The relaxation time  $\tau_i(\vec{q})$  of the two types of deformation can be expressed as<sup>12,13</sup>

$$\frac{1}{\tau_i(\vec{q})} = \frac{K_i q_{\perp}^2 + K_3^2 q_{\parallel}}{\eta_e(\vec{q})}, \quad i = 1, 2 \quad (2)$$

where  $K_1$ ,  $K_2$ , and  $K_3$  are the Frank elastic constants of splay, twist, and bend, respectively; and  $\eta_e(\vec{q})$  is the effective rotational viscosity of the LC with  $q_{\perp}$  denoting the normal component of the wave vector to the LC director  $\hat{n}_0$ , and  $q_{\parallel}$  as the corresponding parallel component. Typically, the fluctuation dynamics in nematic LC is overdamped. The thermally driven fluctuation of the LC director can be described with the hydrodynamic equation of the director field:<sup>14</sup>

$$\eta_e \frac{\partial \hat{n}}{\partial t} = K \nabla^2 \hat{n} - K(\hat{n} \cdot \nabla^2 \hat{n}) \hat{n} \quad (3)$$

with  $K$  denoting an effective elastic constant of LC. For simplicity, we chose the average director orientation  $\hat{n}_0$  to along  $\hat{x}$  and decomposed the thermal fluctuation into two components along  $\hat{y}$  and  $\hat{z}$  as  $\hat{n}(\vec{r}, t) = \hat{x} + n_y(\vec{r}, t) \hat{y} + n_z(\vec{r}, t) \hat{z}$ . Here  $\hat{z}$  is perpendicular to the substrate. To simplify it further, only  $n_y$  is

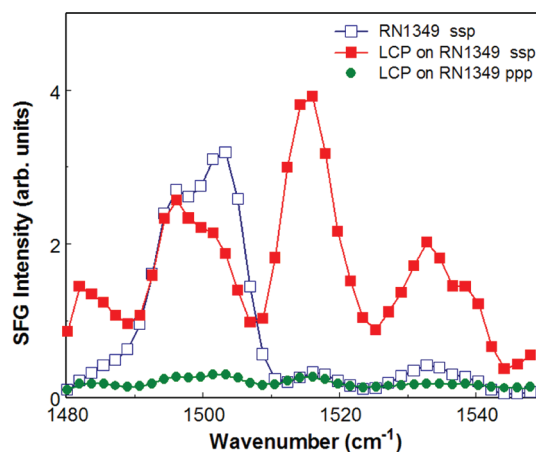


**Figure 4.** SFVS spectra of unexposed RN1349 and LCP on the unexposed film were presented for comparison: open squares (*ssp* spectrum of RN1349), filled squares (*ssp*, LCP/RN1349), filled circles (*ppp*, LCP/RN1349).

taken into account. The boundary condition for the solution is a torque balance condition applied to the cell substrates<sup>15,16</sup>

$$\left( \mp K \frac{\partial n_y}{\partial z} + W n_y + \zeta \frac{\partial n_y}{\partial t} \right) \Big|_{z=0,d} = 0 \quad (4)$$

The first term describes the torque from bulk deformation, which is counter balanced by the surface torque  $W n_y$ , with  $W$  being the anchoring energy strength. When the director is not rigidly anchored to the surfaces, other processes such as adsorption/desorption or molecular slipping on the surface may occur to dissipate the fluctuations. We can include these dissipative effects into  $\zeta \partial n_y / \partial t$  in terms of a phenomenological parameter of surface viscosity  $\zeta$ .

In a nematic LC cell with two equally treated substrates, the orientational fluctuations  $n_y$  have profiles of  $\cos(q_z z)$  and  $\sin(q_z z)$  for even and odd modes, respectively. The corresponding eigenvalue  $q_z$  can be determined from

$$\cot(q_z d) = \frac{K q_z}{2 \left( W - \frac{\zeta}{\tau} \right)} - \frac{W - \frac{\zeta}{\tau}}{2 K q_z} \quad (5)$$

Because the azimuthal fluctuation in LC behaves like a damped relaxation process with a broad distribution of barrier height, we fitted the measured DLS ACF to a stretched exponential

$$g^{(2)}(t) = 1 + \frac{g^{(2)}(0)}{N} \exp[-(t/\tau)^s] \quad (6)$$

to deduce the relaxation time  $\tau$ , which reflects the duration from the correlated to the uncorrelated motion.

## RESULTS AND DISCUSSION

**Vibrational Analysis of the Liquid Crystal Polymer.** To help understanding the measured vibrational characteristics of the LCP layers, we performed an ab initio calculation of biphenyl carbonate, which is the molecular moiety of the system under study.

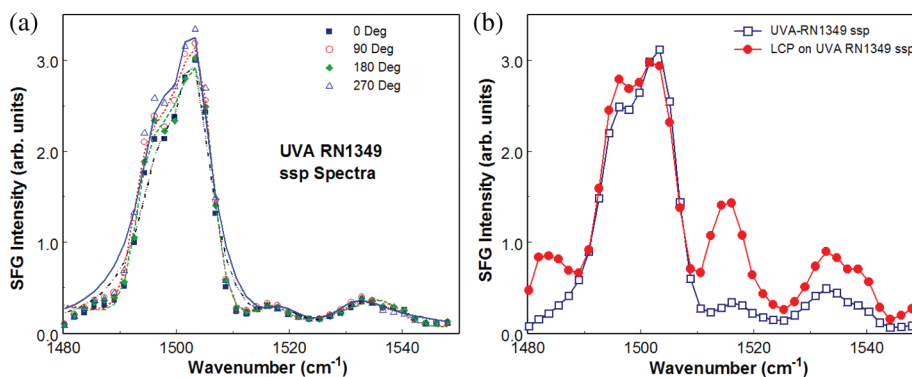


**Figure 5.** (a) *ssp* SFVS spectra of LCP deposited on an LPUV-irradiated RN1349 surface at the C=C stretching region. The spectra were taken with  $E_{UV}$  at  $0^\circ$  (solid squares),  $180^\circ$  (solid diamonds),  $90^\circ$  (open circles), and  $270^\circ$  (open triangles) relative to the incident plane of SFVS measurement. (b) *ssp* SFVS spectra of an LPUV-irradiated RN1349 (open squares) and LCP deposited on the LPUV-irradiated RN1349 surface (solid circles). The lines are the nonlinear least-squares fit to eq 1.

The calculation was carried out with the DMol3 software package,<sup>17</sup> which implements the Perdew–Wang (PW91) generalized gradient approximation (GGA) of density functional theory (DFT) in a double numerical plus polarization (DNP) basis set. The SCF convergence was kept below  $1 \times 10^{-6}$ . The optimized geometry shows that the two phenyl rings connected to the carbonate group are in a *trans* configuration but not lying on the same plane. The ring stretching modes with frequency below  $1500 \text{ cm}^{-1}$  are antisymmetric with IR transition moments perpendicular to the molecular long axis ( $\xi$ ). Between  $1500$  and  $1600 \text{ cm}^{-1}$ , two symmetric ring distortions mixed with C–H wag were found with IR transition moments parallel to the molecular long axis. Other normal modes with symmetric stretch characteristics have vibrational frequencies higher than  $1600 \text{ cm}^{-1}$ . The atom-moving patterns of these ring stretching modes are mostly confined to a single phenyl ring with weak coupling to its neighboring ring. For the SFVS study, we focused on the two symmetric ring distortions between  $1500$  and  $1600 \text{ cm}^{-1}$  in viewing that these two modes not only have an IR transition moment parallel to the molecular long axis, but also possess the character of C–H wags, which may produce significant dynamic dipoles and Raman tensors to yield intense sum frequency generation-active vibrations. In Figure 3, the two symmetric ring distortions are presented. The animated pictures of the normal mode vibrations associated with the core segment can be viewed in the Supporting Information S.2.

**Sum-Frequency Vibrational Spectroscopy of Unirradiated RN1349 and LCP.** We started our experimental SFVS study by first investigating the interaction between RN1349 and LCP layers and then analyzing the orientation of the phenyl ring of LCP. Figure 4 presents the *ssp* SFVS spectra of an RN1349 film without LPUV irradiation (open squares) and an LCP layer deposited on the RN1349 (solid squares). As shown in the figure, the  $1503 \text{ cm}^{-1}$  peak of RN1349 is reduced after depositing a thin layer of LCP. Because SFVS is a sensitive probe for polar structure, the peak reduction suggests that some phenyl groups in the films shall form antiparallely aligned pairs.

To avoid unnecessary complication from RN1349 underlayer, we then focused on the  $1515\text{-cm}^{-1}$  peak, which originates mainly from LCP. We measured the ratio of  $A_{q,ppp}/A_{q,ssp}$  at  $1515 \text{ cm}^{-1}$  to be 0.13. Note that if rings lay flat in the surface plane, the phenylene modes would not be excited by the *ssp* polarization combination. For the LCP film, instead the *ppp* SFVS spectrum

(solid circles) is much weaker than the *ssp* spectrum (solid squares), indicating phenyl groups incline toward the surface. An accurate determination of the orientation of phenyl groups requires a Gaussian distribution  $f(\Omega)$  to be used to take into account a broad angular distribution of  $\Omega$ .<sup>18</sup> Here a rough estimate of the orientation of phenyl groups serves the purpose of further discussion. Therefore, we assumed  $f(\Omega)$  to be a  $\delta$  function. On the basis of a previous SFVS study of the depolarization ratio of the sum-frequency polarizability  $\alpha_{\xi\xi\xi\eta}^{(2)}/\alpha_{\xi\xi\xi\xi}^{(2)} = 0.6$ , with  $\eta$  being the normal direction of the ring plane,<sup>18</sup> the measured  $A_{q,ppp}/A_{q,ssp}$  at  $1515 \text{ cm}^{-1}$  of the LCP yields a polar angle of  $50^\circ$  for the phenyl groups. With the rod-like segment of LCP tilting at  $50^\circ$ , the LCP chains shall be oriented near the surface normal.

**Angle-Resolved SFVS of the LPUV-Defined RN1349 and LCP on the LPUV-irradiated RN1349.** Figure 2a illustrates the configuration of azimuthal angle-resolved SFVS measurement on an LPUV-irradiated film. The resulting *ssp* SFVS spectra are presented in Figure 5a. To more quantitatively deduce the degree of the in-plane alignment of a specific moiety, we defined an in-plane anisotropy  $A = [\chi_{zxx}^{(2)}(\phi = 0^\circ) - \chi_{zyy}^{(2)}(\phi = 90^\circ)]/\chi_{zxx}^{(2)}(\phi = 0^\circ)$  and an in-plane order parameter  $Q = \{2\chi_{zxx}^{(2)}(\phi = 0^\circ)/[\chi_{zxx}^{(2)}(\phi = 0^\circ) + \chi_{zyy}^{(2)}(\phi = 90^\circ)] - 1\}$ .<sup>19</sup> LPUV irradiation on RN1349 yielded  $A = 0.03$  and  $Q = 0.01$  at  $1503 \text{ cm}^{-1}$ , indicating a fairly weak surface anisotropy and alignment order of the phenyl groups in the RN1349 film produced by the LPUV exposure. Figure 5b presents *ssp* SFVS spectra of a LPUV-irradiated RN1349 (open squares) and an LCP deposited on the LPUV-irradiated RN1349 at the C=C stretching region. The spectra were taken with  $E_{UV}$  at  $90^\circ$  relative to the incident plane of the SFVS measurement. It is interesting to note that the signature at  $1503 \text{ cm}^{-1}$  for antiparallely paired phenyl groups in LCP ablates, suggesting that the packing structure of the LCP follows that on the LPUV-irradiated RN1349.

The *ssp* SFVS spectra of LCP films spin-coated with 0.25%, 1%, 2%, 3% and 4% LCP solutions are shown in Figure 6a with  $E_{UV}$  oriented to  $0^\circ$  relative to the incident plane of SFVS. The corresponding spectra taken with  $E_{UV}$  at  $90^\circ$  are presented in Figure 6b. Here the lines are the nonlinear least-squares fit of the SFVS data to eq 1. In Figure 6c, the deduced order parameter  $Q(1515 \text{ cm}^{-1})$  of the LCP films was plotted as a function of LCP thickness. The in-plane order parameter  $Q(1515 \text{ cm}^{-1})$  of the phenyl rings of LCP on LPUV-irradiated RN1349 increases with

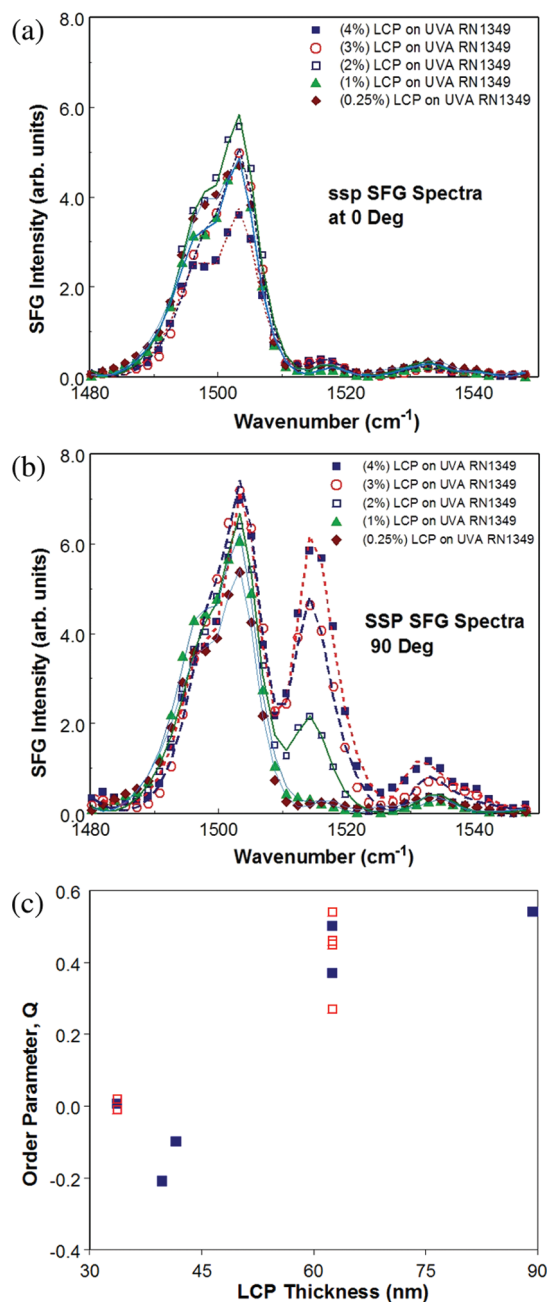


**Figure 6.** *ssp* SFVS spectra of LCP films spin coated with 0.25%, 1%, 2%, 3% and 4% LCP solutions. The polarization of the LPUV light  $E_{UV}$  was oriented at (a)  $0^\circ$  and (b)  $90^\circ$  relative to the incident plane of SFVS measurement. The lines are the nonlinear least-squares fit. (c) The deduced order parameter  $Q$  ( $1515\text{ cm}^{-1}$ ) of the LCP films was plotted as a function of LCP thickness. Multiple data at each layer thicknesses are deduced from different measurements on different samples.

LCP thickness as long as it is larger than 40 nm, suggesting that LCP molecules are aligned in a way similar to an epitaxial growth process. The resulting in-plane order parameter can be as large as 0.6. But in thin LCP layers  $Q(1515\text{ cm}^{-1})$  behaves more complexly, presumably due to counter effects from the LCP self-assembly force and the interaction between the LCP and the photoalignment surfaces.

For the measured SFVS spectra shown in Figure 6b, we found the signal at  $1515\text{ cm}^{-1}$  from the 90-nm thick LCP film to be

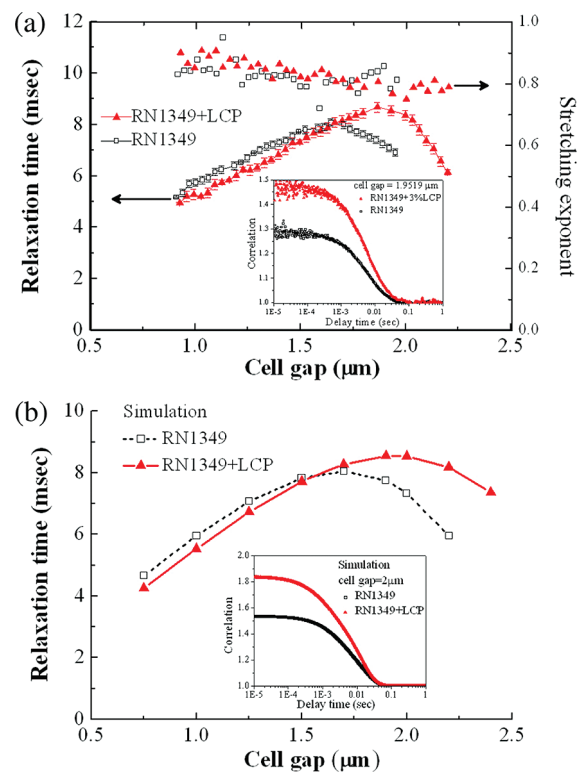


**Figure 7.** The deduced relaxation time and stretching exponent as a function of cell thickness of a wedge cell coated with LCP and LPUV-irradiated RN1349 (filled triangles) and with only LPUV-irradiated RN1349 (open squares). The inset is the measured ACF profiles of the wedge cells at the cell thickness  $d = 1.95\ \mu\text{m}$ , (b) the simulated results for the wedge cell with LCP (filled triangles) and without LCP (open squares). The inset is the corresponding simulated ACF profiles at  $d = 1.95\ \mu\text{m}$ .

about  $1/30$  of the  $z$ -cut  $\text{LiNbO}_3$  reference signal, yielding an SFVS intensity of  $240 \times 10^{-64}\text{ C}^2\text{m}^2/\text{V}^4$ . Assuming the packing density of phenyl ring in LCP is similar to other polymeric films such as poly[4,4'-oxidiphenylenepyrromellitimide] (PMDA-ODA), we estimated that a 45-nm thick LCP layer with polar oriented phenyl rings can generate  $240 \times 10^{-64}\text{ C}^2\text{m}^2/\text{V}^4$  in a reflection geometry. The layer thickness deduced is about one coherence length in a reflection geometry. This result supports the notion that the LCP is grown epitaxially to form a uniaxial structure and the intense SFVS signal originates from the bulk of the LCP layer.

**Dynamic Light Scattering from Liquid Crystal Molecules.** After knowing the azimuthal alignment of the LCP, we expected that the azimuthal anchoring of liquid crystal molecules in contact with LCP layers would be stronger than that on LPUV-irradiated RN1349. To verify this expectation, we employed DLS techniques to probe the dynamic anchoring properties of LC molecules.

We measured the ACF profile of the DLS signal from a liquid crystal wedge cell. We then fit the profiles to eq 6 to deduce the relaxation time  $\tau$  and stretching exponent  $s$ . Figure 7a presents the deduced relaxation time and stretching exponent as a function of LC thickness. We found that at first  $\tau$  increases linearly with LC thickness. After reaching a maximum, the relaxation time decreases, showing that the number of thermal fluctuation modes with wave vector matching to the scattering wave

vector becomes significant.<sup>16</sup> The peak occurs at  $d = 1.95 \mu\text{m}$  for the LC cell with a compound alignment layer, which is larger than that aligned with LPUV-irradiated RN1349 only. In the cell with LCP, a stronger correlation is experienced among the thermally excited fluctuation modes and can persist to larger cell thicknesses before more fluctuation modes are excited to disrupt the correlation.

The stretching exponent  $s$  of the two cells behaves similarly with  $s = 0.9$  at  $d = 0.9 \mu\text{m}$  and decreases slightly to  $0.8$  at  $d = 2.2 \mu\text{m}$ .<sup>16</sup> When more fluctuation modes are excited, a broader distribution of barrier height is yielded. LC molecules have to conquer these barriers in order to reorient, therefore a broader distribution of barrier height causes  $s$  to decrease accordingly. The measured ACFs of the LC wedge cells at  $d = 1.95 \mu\text{m}$  are shown in the inset of Figure 7a. The major difference between the two ACF profiles is the values at short delay time. The measured  $g^{(2)}(0)$  for the cell with LCP is about 1.47 and decreases to 1.28 for the LC cell without LCP. Two effects can change  $g^{(2)}(0)$ . The first one is the randomization effect from multiple fluctuation modes and the other depends on the total number of fluctuating subdomains lying in the optically irradiated region  $N = g^{(2)}(0) / [g^{(2)}(0) - 1]$ . Although the LC cells used for this study were prepared to be single domain, the cells do not thermally fluctuate in unison. By using the measured  $g^{(2)}(0)$  and a light spot of  $20 \mu\text{m}$ , we estimated that in the irradiated region of the cell with LCP there exists three incoherently fluctuating subdomains. Each subdomain has a diameter of  $6 \mu\text{m}$ . While in the cell without LCP, there are about five subdomains and each has a diameter of  $4.5 \mu\text{m}$ . The result supports the picture that a stronger correlation exists in the cell with LCP.

To retrieve the relevant information about the underlying mechanism, we performed a simulation on the two LC wedge cells with eqs 3–5. The results are presented in the Figure 7b. In the simulation, we used a scattering vector of  $q = 2.5 \mu\text{m}^{-1}$ , a surface viscosity  $\zeta = 1 \times 10^{-9} \text{N}\cdot\text{s}/\text{m}$ , and an anchoring energy strength  $W = 3.3 \times 10^{-6} \text{J}/\text{m}^2$ . For the cell aligned with LPUV-irradiated RN1349, the elastic constant was  $K = 9.0 \times 10^{-12} \text{N}$  and viscosity  $\eta = 39 \text{mPa}\cdot\text{s}$ , and for the cell with compound alignment layers of LCP on LPUV-irradiated RN1349,  $K = 2.7 \times 10^{-12} \text{N}$  and  $\eta = 35 \text{mPa}\cdot\text{s}$ . The simulation reproduces all the observed features presented in Figure 7a.  $K$  and  $\eta$  used for the simulation differ for the two cells, reflecting that the viscoelastic characteristics of LC have been changed with a few nanometers thick LCP. The calculated  $g^{(2)}(0)$  is about 1.82 for the cell with compound alignment layers and reduces to 1.54 for the cell aligned only with LPUV-irradiated RN1349. The calculated  $g^{(2)}(0)$  are larger than the measured values, which is mainly due to our simulation considering only the thermal fluctuation modes bound by two substrates. Those subdomain fluctuations in the layer plane were not taken into account.

## CONCLUSIONS

In summary, a simple scheme was developed to transform low alignment order on a LPUV irradiated polymer surface to a desired molecular alignment condition. By employing SFVS, we demonstrated that the weak surface anisotropy of the phenyl ring in the LPUV-irradiated RN1349 layer was printed on a LCP overlayer, and the resulting alignment order of the LCP phenyl rings were improved epitaxially with the layer thickness. DLS techniques further revealed that the viscoelastic properties of the LC molecules were changed by depositing only a few nanometers in thickness of LCP on the LPUV-irradiated RN1349. The method can serve as a convenient toolbox technique, allowing

engineers to optimize the performance of a photonic device by adjusting the boundary forces. The concept could become greatly attractive in the future when device dimensions are reduced to such a scale that the boundary conditions become an important issue.

## ASSOCIATED CONTENT

**S Supporting Information.** Vibrational analysis of biphenyl carbonate moiety and the calibration procedure of SFVS to deduce the absolute magnitude of SFVS susceptibility. This information is available free of charge via the Internet at <http://pubs.acs.org>

## AUTHOR INFORMATION

### Corresponding Author

\*E-mail: [jyhuang@faculty.nctu.edu.tw](mailto:jyhuang@faculty.nctu.edu.tw) Phone: +886 (03)5731975. Fax: +886 (03)5716631.

## ACKNOWLEDGMENT

The authors acknowledge financial support from the Taiwan TFT LCD Association and the National Science Council of the Republic of China under Grant Number NSC97-2112-M009-006-MY3.

## REFERENCES

- (1) Hosono, N.; Kajitani, T.; Fukushima, T.; Ito, K.; Sasaki, S.; Takata, M.; Aida, T. *Science* **2010**, *330*, 808–811.
- (2) Ishihara, S.; Wakemoto, H.; Nakazima, K.; Matsuo, Y. *Liq. Cryst.* **1989**, *4*, 669–675.
- (3) Neil, M. O.; Kelly, S. M. *J. Phys. D* **2000**, *33*, R67.
- (4) Zekonyte, J.; Erichsen, J.; Zaporotchenko, V.; Faupel, F. *Surf. Sci.* **2003**, *532*, 1040–1044.
- (5) Seki, T.; Sakuragi, M.; Kawanishi, Y.; Tamaki, T.; Fukuda, R.; Ichimura, K.; Suzuki, Y. *Langmuir* **1993**, *9*, 211–218.
- (6) Lahann, J.; Mitragotri, S.; Tran, T.-N.; Kaido, H.; Sundaram, J.; Choi, I. S.; Hoffer, S.; Somorjai, G. A.; Langer, R. *Science* **2003**, *299*, 371–374.
- (7) Vidal, F.; Tadjeddine, A. *Rep. Prog. Phys.* **2005**, *68*, 1095–1127 and references therein.
- (8) Wittebrood, M. M.; Rasing, T.; Stallinga, S.; Musevic, I. *Phys. Rev. Lett.* **1998**, *80*, 1232–1235.
- (9) Huang, J. Y.; Shieh, J.-M.; Kuo, H.-C.; Pan, C.-L. *Adv. Funct. Mater.* **2009**, *19*, 2089–2094.
- (10) Wei, X.; Zhuang, X.; Hong, S.-C.; Goto, T.; Shen, Y. R. *Phys. Rev. Lett.* **1999**, *82*, 4256–4259.
- (11) Oh-e, M.; Lvovsky, A. I.; Wei, X.; Shen, Y. R. *J. Chem. Phys.* **2000**, *113*, 8827–8832.
- (12) de Gennes, P. G.; Prost, J. *The Physics of Liquid Crystals*; Clarendon: Oxford, 1993.
- (13) Vilfan, M.; Mertelj, A.; Copic, M. *Phys. Rev. E* **2002**, *65*, 041712.
- (14) Kelly, J. R.; Palffy-Muhoray, P. *Phys. Rev. E* **1997**, *55*, 4378–4381.
- (15) Mertelj, A.; Copic, M. *Phys. Rev. E* **2000**, *61*, 1622–1628.
- (16) Vilfan, M.; Olenik, I. D.; Mertelj, A.; Copic, M. *Phys. Rev. E* **2001**, *63*, 061709.
- (17) DMol3 package of the Materials Studio software environment; Accelrys (<http://accelrys.com/>).
- (18) Oh-e, M.; Hong, S.-C.; Shen, Y. R. *Appl. Phys. Lett.* **2002**, *80*, 784–786.
- (19) Ouchi, Y.; Feller, M. B.; Moses, T.; Shen, Y. R. *Phys. Rev. Lett.* **1992**, *68*, 3040–3043.